

Chirality of Valley Excitons in Monolayer Transition-Metal Dichalcogenides

Fabio Caruso,^{*,†} Maximilian Schebek,[‡] Yiming Pan,[†] Cecilia Vona,[‡] and Claudia
Draxl[‡]

[†]*Institut für Theoretische Physik und Astrophysik, Christian-Albrechts-Universität zu Kiel,
Kiel, Germany*

[‡]*Institut für Physik and IRIS Adlershof, Humboldt-Universität zu Berlin, Berlin, Germany*

E-mail: caruso@physik.uni-kiel.de

Abstract

By enabling control of valley degrees of freedom in transition-metal dichalcogenides, valley-selective circular dichroism has become a key concept in valleytronics. In this manuscript, we show that valley excitons – bound electron-hole pairs formed at either the K or \bar{K} valleys upon absorption of circularly-polarized light – are chiral quasiparticles characterized by a finite orbital angular momentum (OAM). We further formulate an *ab-initio* many-body theory of valley-selective circular dichroism and valley excitons based on the Bethe-Salpeter equation. Beside governing the interaction with circularly polarized light, the OAM confers excitons a finite magnetization which manifests itself through an excitonic Zeeman splitting upon interaction with external magnetic fields. The good agreement between our *ab-initio* calculations and recent experimental measurements of the exciton Zeeman shifts corroborate this picture.

Introduction

The two-fold valley degeneracy of monolayer transition-metal dichalcogenides (TMDs) makes them suitable candidates for the exploration of novel concepts in valleytronics¹. The rich valley physics of the TMDs manifests itself, for instance, in the formation of valley excitons², chiral phonons³, nonequilibrium phonon populations⁴, as well as non-trivial topological properties⁵, which are exemplified by the emergence of Hall effects in various flavors^{6–9}, and valley-dependent optical selection rules^{10,11}.

Circularly-polarized light can lead to a pronounced valley-selective circular dichroism (VCD)^{12–19}, whereby absorption is governed by the formation of bound electron-hole pairs (excitons) at either the K or \bar{K} valleys in the Brillouin zone (BZ) depending on the light helicity. VCD enables to selectively tailor the population of excitons and excited carriers in the BZ, and it has opened new promising venues to achieve properties on demand using light²⁰. Additionally, the exploitation of valley degrees of freedoms in TMDs relies on the possibility to establish an imbalance in the population of the K and \bar{K} valleys. Thus, the concept of VCD has become a central ingredient for valleytronics applications involving TMDs²¹, and it has provided a strong stimulus for experimental research^{22–25}.

The emergence of VCD has been ascribed to the lack of an inversion center in the hexagonal lattice of TMDs monolayers^{5,10}, which leads to finite and opposite Berry curvatures and orbital angular momenta at the K and \bar{K} valleys. Earlier theoretical studies of circular dichroism rely on the single-particle picture, whereby the ties between dichroic absorption, Berry curvature, and orbital magnetization can be rigorously established^{26–33}. Despite the remarkable progress in understanding the interplay between topological properties and circular dichroism, the single-particle picture is unsuitable to account for the formation of valley excitons – which are inherently two-particle excitations –, as well as for the non-trivial response of valley excitons to external perturbations reported in recent experimental investigations. The presence of an external magnetic field leads to the valley Zeeman effect, whereby the degeneracy of valley excitons is lifted and the ensuing energy shift is linear in the

field intensity^{6,34}. In presence of an in-plane electric field, valley excitons are subject to the exciton Hall effect, a drift velocity transversal to field orientation which is reminiscent of the anomalous Hall effect^{8,35}. Overall, these findings suggest that valley excitons may possess an additional orbital degree of freedom governing its interaction with external perturbation and their topological properties.

In this manuscript, we formulate an *ab-initio* many-body theory of valley excitons and valley-selective circular dichroism based on the Bethe-Salpeter equation (BSE). Our approach provides a new route to accurately predict the degree of valley polarization upon absorption of circularly polarized light in an interacting electron-hole gas. It is further shown that valley excitons formed in TMDs monolayers at either the K or \bar{K} valley upon VCD exhibit a non-trivial chirality. In particular, valley excitons are characterized by a finite orbital angular momentum, which is inherited by the underlying band structure, and provides a new rationale to explain the emergence of VCD in interacting electron systems. The OAM confers excitons a finite magnetic moment that, in concomitance with an external magnetic field, underpins a Zeeman-like splitting of the excitonic peaks.

Results

For definiteness, we focus in the following on monolayer WS₂, although similar conclusions can be drawn also for WSe₂, MoS₂, and MoSe₂. Monolayer WS₂ is a direct band-gap semiconductor³⁶ and its valence band is characterized by two degenerate maxima at K and \bar{K} . The hexagonal BZ and the energy of the upper valence band are illustrated in Fig. 1 (a) and (b), respectively. To investigate the influence of light polarization on the bound excitons formed at the K and \bar{K} valleys, we solve the many-body BSE, and consider the imaginary part ε_2 of the transverse dielectric function $\varepsilon = \varepsilon_1 + i\varepsilon_2$ ³⁷:

$$\varepsilon_2(\omega) = \frac{4\pi^2 e^2}{m_e^2 \Omega N_k} \sum_{\lambda} |\hat{\mathbf{e}} \cdot \mathbf{t}^{\lambda}|^2 \delta(E^{\lambda} - \hbar\omega) \quad . \quad (1)$$

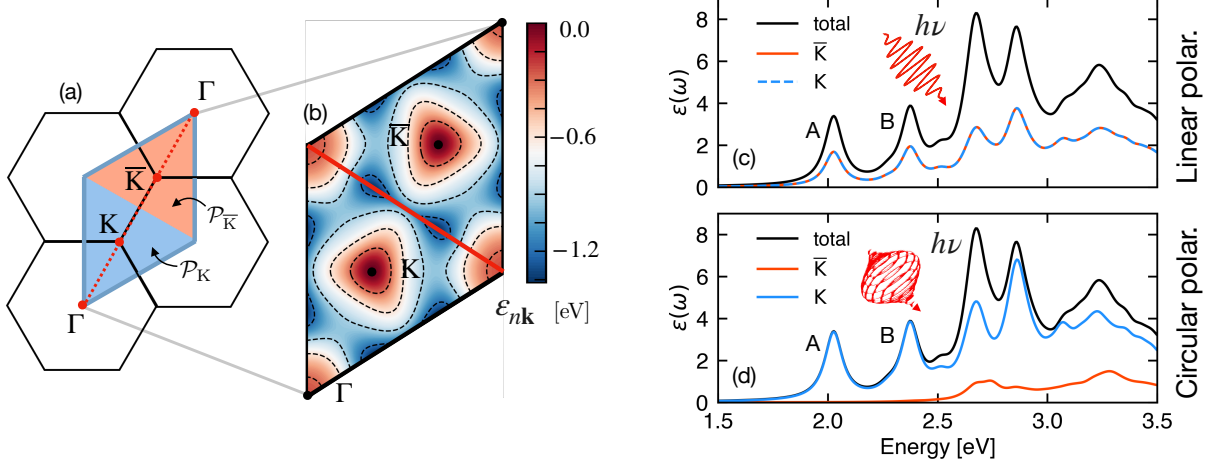


Figure 1: (a) Brillouin zone and high-symmetry points of monolayer WS_2 . The blue and orange shadings mark the \mathcal{P}_K and $\mathcal{P}_{\bar{K}}$ regions in the BZ, respectively. The path Γ -K-M- \bar{K} - Γ is shown as a dotted red line. (b) Energy (relative to the valence-band top) of the upper valence band for momenta in the rhomboidal BZ. The red continuous line delimits the two inequivalent regions of the BZ, containing the K and \bar{K} valleys. (c-d) Total absorption spectrum as obtained from the solution of the BSE (black), and contribution of the inequivalent K (blue) and \bar{K} (orange) valleys to the absorption for the cases of linear (c) and circular light polarization (d) with left-handed chirality. A and B denote the lower and higher-energy excitonic peaks, respectively.

Here, $\hat{\epsilon}$ denotes the light-polarization unitary vector, Ω the unit cell volume, and N_k the number of k-points. The transition coefficients \mathbf{t}_λ are defined as:

$$\mathbf{t}^\lambda = \sum_{vc} \sum_{\mathbf{k}}^{\text{BZ}} A_{vc\mathbf{k}}^\lambda \frac{\langle \psi_{v\mathbf{k}} | \hat{\mathbf{p}} | \psi_{c\mathbf{k}} \rangle}{\epsilon_{c\mathbf{k}} - \epsilon_{v\mathbf{k}}}, \quad (2)$$

where $\hat{\mathbf{p}}$ is the momentum operator, $\psi_{n\mathbf{k}}$ and $\epsilon_{n\mathbf{k}}$ are single-particle Bloch orbitals and energies, respectively, and the sum over v (c) runs over the valence (conduction) bands. E^λ and $A_{vc\mathbf{k}}^\lambda$ are the eigenvalues and eigenvectors³⁷, respectively, obtained from the diagonalization of the two-particle BSE Hamiltonian $\sum_{v'c'\mathbf{k}'} H_{vc\mathbf{k},v'c'\mathbf{k}'} A_{v'c'\mathbf{k}'}^\lambda = E^\lambda A_{vc\mathbf{k}}^\lambda$.

The dielectric function evaluated from Eq. (1) is illustrated in Fig. 1 (c-d) in black. As long as the *total* absorption is considered – i.e., electronic transitions in the whole BZ (as opposed to the valley-dependent absorption within a specific valley) – the dielectric function of WS_2 is independent of the light-polarization vector $\hat{\epsilon}$. The absorption onset is dominated

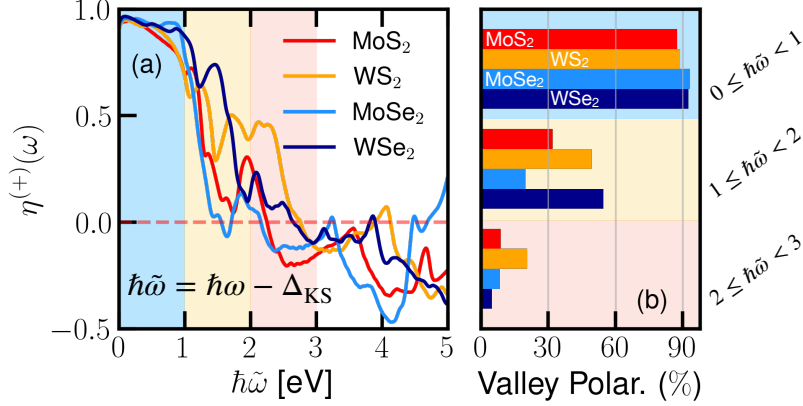


Figure 2: (a) Degree of valley polarization $\eta^{(+)}$ induced by left-handed circularly-polarized light in WS₂, MoS₂, MoSe₂, and WSe₂. Energies are relative to the Kohn-Sham band gap Δ_{KS} . (b) Average valley polarization for photon energies ranging between 0 and 1 eV (top), 1 and 2 eV (center), 2 and 3 eV (bottom) above the absorption onset.

by strongly-bound excitons localized at K and $\bar{\text{K}}$, marked as A and B in Fig. 1 (c) and (d), in good agreement with earlier calculations and experiments^{38,39}.

To investigate the role played by the inequivalent K and $\bar{\text{K}}$ valleys in the absorption of polarized light, we partition the BZ into two regions \mathcal{P}_{K} and $\mathcal{P}_{\bar{\text{K}}}$, shaded in Fig. 1 (a), which enclose K and $\bar{\text{K}}$, respectively. Next, we consider the valley-resolved transition coefficients $\mathbf{t}_{\text{K}}^{\lambda}$ ($\mathbf{t}_{\bar{\text{K}}}^{\lambda}$), defined by restricting the sum over momenta in Eq. (2) to the \mathcal{P}_{K} ($\mathcal{P}_{\bar{\text{K}}}$) region in reciprocal space, (i.e., replacing $\sum_{\mathbf{k}}^{\text{BZ}}$ with $\sum_{\mathbf{k}}^{\mathcal{P}_{\text{K}}}$). Additivity follows straightforwardly from these definitions ($\mathbf{t}^{\lambda} = \mathbf{t}_{\text{K}}^{\lambda} + \mathbf{t}_{\bar{\text{K}}}^{\lambda}$). We define the valley-resolved dielectric function $\varepsilon_{2,\text{K}}$ ($\varepsilon_{2,\bar{\text{K}}}$) by retaining only the valley-resolved transition coefficients in the evaluation of Eq. (1). In short, $\varepsilon_{2,\text{K}}$ ($\varepsilon_{2,\bar{\text{K}}}$) accounts for absorption processes resulting exclusively from the excitation of electron-hole pairs within the K ($\bar{\text{K}}$) valley, and to a good approximation the identity $\varepsilon_2(\omega) \approx \varepsilon_{2,\text{K}}(\omega) + \varepsilon_{2,\bar{\text{K}}}(\omega)$ holds for frequencies in the vicinity of the absorption onset (see Supplementary Fig. S2⁴⁰). For left- (+) and right-handed (-) circular polarization, the light-polarization vector $\hat{\mathbf{e}}$ can be expressed as⁴¹: $\hat{\mathbf{e}}_{\pm} = (\hat{\mathbf{x}} \pm i\hat{\mathbf{y}})/\sqrt{2}$, where $\hat{\mathbf{x}}$ and $\hat{\mathbf{y}}$ are Cartesian unit vectors. By accounting explicitly for the circular polarization via the unitary vectors $\hat{\mathbf{e}}_{\pm}$, one promptly obtains an explicit expression for the imaginary part of

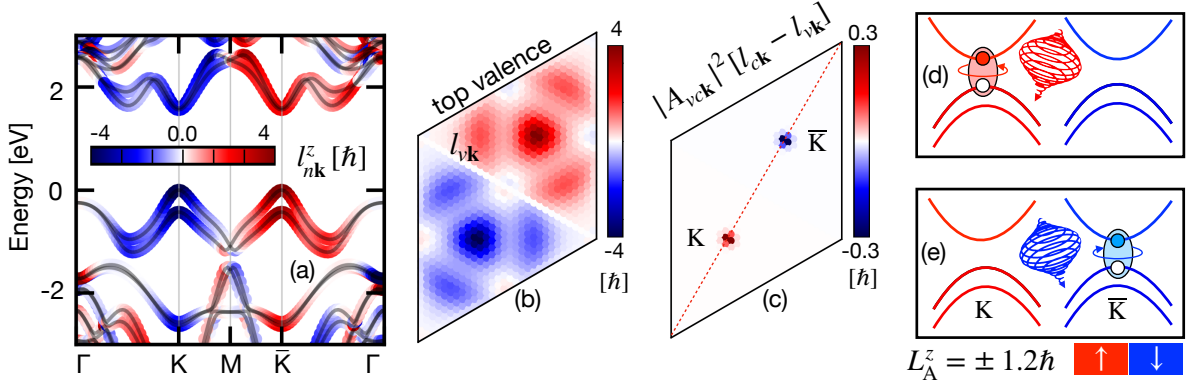


Figure 3: (a) Orbital angular momentum $l_{nk\sigma}^z$ superimposed to the band structure of monolayer WS_2 for momenta along the Γ -K-M- $\bar{\text{K}}$ - Γ line. (b) OAM for the top valence band for momenta in the BZ. (c) Momentum-resolved contribution to the OAM of valley excitons. (d) Schematic illustration of valley-selective circular dichroism and chiral valley excitons in the TMDs.

the transverse dielectric function at K for circularly-polarized light:

$$\varepsilon_{2,\text{K}}^{(\pm)}(\omega) = \frac{1}{2} [\xi_{xx}^{\text{K}}(\omega) + \xi_{yy}^{\text{K}}(\omega)] \mp \text{Im} [\xi_{xy}^{\text{K}}(\omega)] \quad , \quad (3)$$

where we introduced the *dichroic tensor*: $\xi_{\text{K}}^{\alpha\beta}(\omega) = \frac{4\pi^2 e^2}{m_e^2 \Omega N_{\text{K}}} \sum_{\lambda} \left(t_{\text{K}}^{\lambda,\alpha} \right)^* t_{\text{K}}^{\lambda,\beta} \delta(E^{\lambda} - \hbar\omega)$. The corresponding expression for $\bar{\text{K}}$ is obtained by replacing $\text{K} \rightarrow \bar{\text{K}}$. A detailed discussion of these expression is included in the SI⁴⁰.

The emergence of valley-selective circular dichroism can be quantified by introducing the differential dichroic absorption:

$$D_{\text{K}}(\omega) = \varepsilon_{2,\text{K}}^{(+)}(\omega) - \varepsilon_{2,\text{K}}^{(-)}(\omega) = -2\text{Im} [\xi_{\text{K}}^{xy}(\omega)]. \quad (4)$$

In monolayer WS_2 , the *total* off-diagonal components of the dichroic tensor vanish at all frequencies ($\xi^{xy}(\omega) = \xi_{\text{K}}^{xy}(\omega) + \xi_{\bar{\text{K}}}^{xy}(\omega) = 0$), leading in turn to a vanishing differential dichroic absorption ($D(\omega) = D_{\text{K}} + D_{\bar{\text{K}}} = 0$). The total absorption spectrum is thus ultimately independent of the helicity of light polarization. Conversely, the valley-resolved components of the dichroic tensor are finite and opposite in sign at K and $\bar{\text{K}}$ ($\text{Im} [\xi_{\text{K}}^{xy}] = -\text{Im} [\xi_{\bar{\text{K}}}^{xy}] \neq 0$)

indicating that, despite the total vanishing dichroism, the individual valleys are characterized by a non-trivial chiral character, leading to a non-vanishing differential dichroic absorption.

To analyze these phenomena on a quantitative ground, we proceed to investigate the optical response of the K and \bar{K} valleys to light with different polarization states. For *linear* polarization, we consider for definiteness a polarization vector $\hat{\mathbf{e}} = \hat{\mathbf{x}}$. The absorption in the K and \bar{K} valleys is thus described by the xx component of the corresponding valley-resolved dielectric tensors, i.e., $\varepsilon_{2,K}^{xx}$ and $\varepsilon_{2,\bar{K}}^{xx}$, which are reported in Fig. 1 (c), in orange and blue (dashed), respectively. The overlap of $\varepsilon_{2,K}^{xx}$ and $\varepsilon_{2,\bar{K}}^{xx}$ for all photon energies reflects the identical response of carriers in the K and \bar{K} valleys: light absorption is equally likely to be mediated by optical excitations at K or \bar{K} .

The situation is qualitatively different when circular polarization is considered. For left-handed polarization, the valley-resolved dielectric functions $\varepsilon_{2,K}^{(+)}$ and $\varepsilon_{2,\bar{K}}^{(+)}$ – evaluated from Eq. (3) and illustrated in Fig. 1 (d) – indicate a strikingly different optical response at K and \bar{K} . The absorption onset is dominated by pronounced excitonic peaks in the \mathcal{P}_K region of the BZ, whereas optical excitations in $\mathcal{P}_{\bar{K}}$ are virtually suppressed at the absorption onset, giving a sizeable contribution only at energies larger than the fundamental gap. Correspondingly, light is almost exclusively absorbed in the \mathcal{P}_K region of the BZ in the vicinity of the absorption onset. These findings reflect the formation of valley excitons at K , and the absence of excitonic states at \bar{K} . The scenario is reversed if the degree of circular polarization is inverted (not shown).

To assess the degree of valley selectivity in the absorption of polarized light, we define the degree of valley polarization η for left-handed polarization (+),

$$\eta^{(+)}(\omega) = \frac{\varepsilon_{2,K}^{(+)} - \varepsilon_{2,\bar{K}}^{(+)}}{\varepsilon_{2,K}^{(+)} + \varepsilon_{2,\bar{K}}^{(+)}} . \quad (5)$$

For right-handed polarization (–) one easily finds $\eta^{(-)} = -\eta^{(+)}$. For a given photon frequency ω , η assumes values in the range $[-1, 1]$, where $\eta(\omega) = 0$ denotes absence of valley polarization

and $\eta(\omega) = \pm 1$ indicates complete valley polarization. Figure 2 (a) illustrates values of $\eta^{(+)}$ evaluated in the independent particle approximation (IPA) for WS₂, and the TMDs MoS₂, MoSe₂, and WSe₂ in their hexagonal monolayer structure. The valley polarization η evaluated in the IPA is found to agree well with the result of BSE calculations, as shown in Fig.S3. For all compounds, the degree of valley polarization approaches unity in the vicinity of the absorption onset, and it decreases rapidly for increasing photon energies. Figure 2 (b) reports the average valley polarization for photon energies in the vicinity of the absorption onset (0-1 eV, blue shading in Fig. 2 (a)), and at larger frequencies (1-2 eV in orange shading, and 2-3 eV in red shading). For WS₂, on average valley polarization of 89% is obtained for energies up to 1 eV above the fundamental gap. This value agrees well with the experimental estimate of 84% obtained by time-resolved ARPES measurements of the valence band¹⁸. Valley polarization exceeding 90% may be obtained in WSe₂ and MoSe₂. These values constitute a theoretical upper limit for the degree of valley polarization.

In the following, we proceed to inspect the chiral character of valley excitons via *ab-initio* calculation of the exciton OAM. The wave function of an excitonic state λ can be expressed in terms of the eigenstates of the BSE Hamiltonian $A_{v\mathbf{c}\mathbf{k}}^\lambda$ as $|\lambda\rangle = \sum_{v\mathbf{c}\mathbf{k}} A_{v\mathbf{c}\mathbf{k}}^\lambda |\psi_{v\mathbf{k}}^h \psi_{\mathbf{c}\mathbf{k}}^e\rangle$, where $\psi_{\mathbf{c}\mathbf{k}}^e$ and $\psi_{v\mathbf{k}}^h$ denote the Bloch orbitals of electrons and holes, respectively. By considering the OAM operator for an electron-hole pair $\hat{\mathbf{L}} \equiv \hat{\mathbf{l}}_e + \hat{\mathbf{l}}_h$, with $\hat{\mathbf{l}}_{e(h)} = \hat{\mathbf{r}}_{e(h)} \times \hat{\mathbf{p}}_{e(h)}$, we obtain an explicit expression for the out-of-plane component of the OAM of the exciton λ :

$$L_\lambda^z = \langle \lambda | \hat{L}^z | \lambda \rangle = \sum_{v\mathbf{c}\mathbf{k}} |A_{v\mathbf{c}\mathbf{k}}^\lambda|^2 [l_{\mathbf{c}\mathbf{k}}^z - l_{v\mathbf{k}}^z] \quad . \quad (6)$$

The derivation of Eq. (6) is discussed in detail in the SI⁴⁰. $l_{n\mathbf{k}}^z$ denotes the single-particle OAM for a Bloch state $\psi_{n\mathbf{k}}$, and it is given by²⁸:

$$l_{n\mathbf{k}}^z = \frac{2\hbar}{m_e} \sum_{m \neq n} \frac{\text{Im} [M_{nm}^x M_{mn}^y]}{\varepsilon_{m\mathbf{k}} - \varepsilon_{n\mathbf{k}}} \quad , \quad (7)$$

with the abbreviation $M_{nm}^\alpha = \langle \psi_{n\mathbf{k}} | \hat{p}^\alpha | \psi_{m\mathbf{k}} \rangle$. The single-particle OAM, evaluated from

Eq. (7), is shown in Fig. 3(a) as a color code superimposed to the band structure of WS₂. The lower and upper valence bands exhibit the largest OAM, with opposite sign at the K and \bar{K} points. The single-particle OAM of the top valence band is further illustrated in Fig. 3(b). The total OAM of each valley, obtained from $l_{\bar{K}}^z = \int_{\mathcal{P}_{\bar{K}}} l_{v\mathbf{k}} d\mathbf{k}$, yields $l^z = \pm 0.7 \hbar$.

These considerations indicate that excitons inherit the OAM from the underlying band structure. Upon absorption of linearly polarized light, however, the exciton OAM vanishes identically owing to the compensating contribution from K and \bar{K} . To illustrate this point, we report in Fig. 3(c) the momentum-resolved contribution to the OAM of the A exciton, obtained from the expression $|A_{v\mathbf{c}\mathbf{k}}^\lambda|^2 [l_{c\mathbf{k}}^z - l_{v\mathbf{k}}^z]$ (see also Eq. (6)). Conversely, in presence of circularly-polarized light, excitons are localized at either K or \bar{K} , no compensation occurs, and *chiral excitons* characterized by a finite OAM can emerge. More precisely, the prerequisite for the emergence of chiral excitons is the OAM of the valence and conduction manifold to differ for band indices c, v and momenta \mathbf{k} contributing to the exciton formation (that is, $l_{c\mathbf{k}} \neq l_{v\mathbf{k}}$ for $A_{v\mathbf{c}\mathbf{k}}^\lambda \neq 0$). This condition is satisfied by valley excitons localized exclusively at K or \bar{K} . Evaluation of Eq. (6) yields $L_{\bar{A}}^z = \pm 1.2 \hbar$ for A valley excitons at K and \bar{K} , whereas for the B exciton we obtain $L_{\bar{B}}^z = \pm 1.0 \hbar$. Because valley excitons are formed by electron-hole pairs in the vicinity of K (\bar{K}) to a good approximation one has $L_{\lambda\bar{K}}^z \simeq l_{c\mathbf{K}} - l_{v\mathbf{K}}$. The minus sign reflects the momentum reversal for holes (see SI⁴⁰).

The concept of OAM provides a valuable tool to unravel the microscopic origin of valley dichroism in TMDs. In the independent-particle approximation, the dichroic sum rule^{28,29} indicates that circular dichroism is a manifestation of the finite OAM of independent electrons in the sample. While we were unable to derive an exact sum rule relating the exciton OAM and the differential dichroic absorption in the interacting picture, a simple relation between these quantities can be established for a two-level system (see SI⁴⁰), suggesting that valley dichroism is a direct manifestation of the exciton chirality.

The presence of a finite OAM further confers excitons an orbital magnetic moment $M_\lambda^z = -(e/2m_e)L_\lambda^z$, which in turn provides a route for the interaction of excitons with

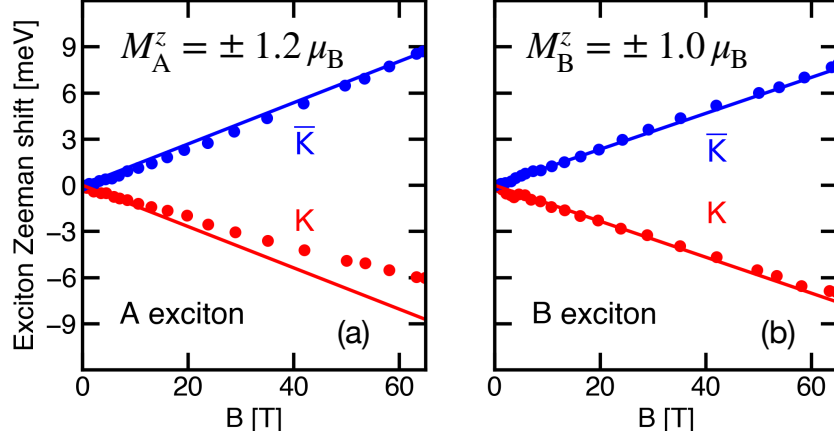


Figure 4: *Ab-initio* exciton Zeeman shifts for the A (a) and B excitons (b) as a function of external magnetic field (lines). Experimental data (dots) are reproduced from Ref.⁴⁴.

external magnetic fields and other spin-orbital degrees of freedom. The presence of an external magnetic field in concomitance with finite and opposite orbital magnetic moment M_λ^z is expected to lift the degeneracy of valley excitons at K and \bar{K} , leading to a Zeeman shift of their energy according to $\Delta E_b = -\mathbf{M}_\lambda \cdot \mathbf{B}$. The shift of exciton peaks in the absorption spectrum of TMDs in presence of external magnetic fields has been observed in recent experimental magneto-optical studies^{42–46}. We illustrate in Fig. 4 *ab-initio* exciton Zeeman shifts ΔE_b for WS₂ as a function of external fields (lines), alongside with magneto-reflectance spectroscopy data from Ref.⁴⁴ (dots). The excellent agreement between theory and experimental data in Fig. 4 corroborates our findings and it provides further evidence in support of the orbital degree of freedom of valley excitons in transition-metal dichalcogenides. These results further suggests that photo-luminescence magneto-reflectance spectroscopy constitutes a suitable tool to directly probe the OAM and orbital magnetic moment of excitons.

Conclusions

In conclusion, we presented a first-principles theory of valley-selective circular dichroism and valley excitons in monolayer WS₂ based on many-body perturbation theory and the BSE.

We showed that valley excitons formed upon absorption of circularly-polarized light and localized at either the K or \bar{K} valley in the BZ, are chiral quasiparticles characterized by finite orbital angular momentum and orbital magnetic moment. This picture is validated via *ab-initio* calculations of the exciton Zeeman splitting in good agreement with recent experimental studies. More generally, the orbital angular momentum constitutes an internal degree of freedom of valley excitons that influences selection rules, the coupling to external perturbations and other spin-orbital degrees of freedom, and it provides a promising concept to unravel the recently discovered topological behaviour of excitons^{8,35}.

Methods

Computational details

Optical properties have been computed using the full-potential all-electron code `exciting`^{47,48}. For both species, muffin tin radii of 2.2 Bohr have been used with a basis set cut-off of $R_{\text{MT}}|\mathbf{G} + \mathbf{k}|_{\text{max}} = 8.0$. A grid of $30 \times 30 \times 1$ \mathbf{k} -points was employed for the calculations, local-field effects were included up to a cut-off of $|\mathbf{G} + \mathbf{q}|_{\text{max}} = 3.0 \text{ Bohr}^{-1}$. The PBE exchange-correlation functional⁴⁹ was used to compute the Kohn-Sham states, 100 unoccupied states were included in the calculation of the dielectric matrix, spin-orbit coupling was accounted for through the second variation approach. Four valence and four conduction bands have been considered in the solution of the BSE, and a broadening of 50 meV has been applied in the computation of the dielectric function. The orbital magnetization has been computed using a modified version of the `epsilon.x` program, part of `Quantum Espresso`.

Acknowledgments

This project has been funded by the Deutsche Forschungsgemeinschaft (DFG) – project numbers 443988403, 424709454, and 182087777. Discussions with Michael Bauer are grate-

fully acknowledged. MS acknowledges support by the IMPRS for Elementary Processes in Physical Chemistry.

References

- (1) Rycerz, A.; Tworzydło, J.; Beenakker, C. W. J. Valley filter and valley valve in graphene. *Nat. Phys.* **2007**, *3*, 172–175.
- (2) Yu, H.; Cui, X.; Xu, X.; Yao, W. Valley excitons in two-dimensional semiconductors. *Natl. Sci. Rev.* **2015**, *2*, 57–70.
- (3) Zhu, H.; Yi, J.; Li, M.-Y.; Xiao, J.; Zhang, L.; Yang, C.-W.; Kaindl, R. A.; Li, L.-J.; Wang, Y.; Zhang, X. Observation of chiral phonons. *Science* **2018**, *359*, 579–582.
- (4) Caruso, F. Nonequilibrium Lattice Dynamics in Monolayer MoS₂. *J. Phys. Chem. Lett* **2021**, *12*, 1734–1740.
- (5) Yao, W.; Xiao, D.; Niu, Q. Valley-dependent optoelectronics from inversion symmetry breaking. *Phys. Rev. B* **2008**, *77*, 235406.
- (6) Mak, K. F.; McGill, K. L.; Park, J.; McEuen, P. L. The valley Hall effect in MoS₂ transistors. *Science* **2014**, *344*, 1489–1492, 00000.
- (7) Qian, X.; Liu, J.; Fu, L.; Li, J. Quantum spin Hall effect in two-dimensional transition metal dichalcogenides. *Science* **2014**, *346*, 1344–1347.
- (8) Onga, M.; Zhang, Y.; Ideue, T.; Iwasa, Y. Exciton Hall effect in monolayer MoS₂. *Nat. Mater.* **2017**, *16*, 1193–1197.
- (9) Dau, M. T.; Vergnaud, C.; Marty, A.; Beigné, C.; Gambarelli, S.; Maurel, V.; Journot, T.; Hyot, B.; Guillet, T.; Grévin, B.; Okuno, H.; Jamet, M. The valley Nernst effect in WSe₂. *Nat. Commun.* **2019**, *10*, 5796.

- (10) Xiao, D.; Liu, G.-B.; Feng, W.; Xu, X.; Yao, W. Coupled Spin and Valley Physics in Monolayers of MoS₂ and Other Group-VI Dichalcogenides. *Phys. Rev. Lett.* **2012**, *108*, 196802.
- (11) Cao, T.; Wu, M.; Louie, S. G. Unifying Optical Selection Rules for Excitons in Two Dimensions: Band Topology and Winding Numbers. *Phys. Rev. Lett.* **2018**, *120*, 087402.
- (12) Cao, T.; Wang, G.; Han, W.; Ye, H.; Zhu, C.; Shi, J.; Niu, Q.; Tan, P.; Wang, E.; Liu, B.; Feng, J. Valley-selective circular dichroism of monolayer molybdenum disulphide. *Nat. Commun.* **2012**, *3*, 887.
- (13) Mak, K. F.; He, K.; Shan, J.; Heinz, T. F. Control of valley polarization in monolayer MoS₂ by optical helicity. *Nat. Nanotechnol.* **2012**, *7*, 494–498.
- (14) Zeng, H.; Dai, J.; Yao, W.; Xiao, D.; Cui, X. Valley polarization in MoS₂ monolayers by optical pumping. *Nat. Nanotechnol.* **2012**, *7*, 490–493.
- (15) Jones, A. M.; Yu, H.; Ghimire, N. J.; Wu, S.; Aivazian, G.; Ross, J. S.; Zhao, B.; Yan, J.; Mandrus, D. G.; Xiao, D.; Yao, W.; Xu, X. Optical generation of excitonic valley coherence in monolayer WSe₂. *Nat. Nanotechnol.* **2013**, *8*, 634–638.
- (16) Mak, K. F.; He, K.; Lee, C.; Lee, G. H.; Hone, J.; Heinz, T. F.; Shan, J. Tightly bound trions in monolayer MoS₂. *Nat. Mater.* **2013**, *12*, 207–211.
- (17) Mak, K. F.; Shan, J. Photonics and optoelectronics of 2D semiconductor transition metal dichalcogenides. *Nat. Photon.* **2016**, *10*, 216–226.
- (18) Beyer, H.; Rohde, G.; Grubišić Čabo, A.; Stange, A.; Jacobsen, T.; Bignardi, L.; Lizzit, D.; Lacovig, P.; Sanders, C.; Lizzit, S.; Rossnagel, K.; Hofmann, P.; Bauer, M. 80% Valley Polarization of Free Carriers in Singly Oriented Single-Layer WS₂ on Au(111). *Phys. Rev. Lett.* **2019**, *123*, 236802.

- (19) Beaulieu, S.; Schusser, J.; Dong, S.; Schüler, M.; Pincelli, T.; Dendzik, M.; Maklar, J.; Neef, A.; Ebert, H.; Hricovini, K.; Wolf, M.; Braun, J.; Rettig, L.; Minár, J.; Ernstorfer, R. Revealing Hidden Orbital Pseudospin Texture with Time-Reversal Dichroism in Photoelectron Angular Distributions. *Phys. Rev. Lett.* **2020**, *125*, 216404.
- (20) Basov, D. N.; Averitt, R. D.; Hsieh, D. Towards properties on demand in quantum materials. *Nat. Mater.* **2017**, *16*, 1077–1088.
- (21) Mak, K. F.; Xiao, D.; Shan, J. Light–valley interactions in 2D semiconductors. *Nat. Photon.* **2018**, *12*, 451–460.
- (22) Mai, C.; Barrette, A.; Yu, Y.; Semenov, Y. G.; Kim, K. W.; Cao, L.; Gundogdu, K. Many-Body Effects in Valleytronics: Direct Measurement of Valley Lifetimes in Single-Layer MoS₂. *Nano Lett.* **2014**, *14*, 202–206.
- (23) Wu, S.; Ross, J. S.; Liu, G.-B.; Aivazian, G.; Jones, A.; Fei, Z.; Zhu, W.; Xiao, D.; Yao, W.; Cobden, D.; Xu, X. Electrical tuning of valley magnetic moment through symmetry control in bilayer MoS₂. *Nat. Phys.* **2013**, *9*, 149–153.
- (24) Zhang, Y. J.; Oka, T.; Suzuki, R.; Ye, J. T.; Iwasa, Y. Electrically Switchable Chiral Light-Emitting Transistor. *Science* **2014**, *344*, 725–728.
- (25) Scuri, G. et al. Electrically Tunable Valley Dynamics in Twisted WSe₂ / WSe₂ Bilayers. *Phys. Rev. Lett.* **2020**, *124*, 217403.
- (26) Thole, B. T.; Carra, P.; Sette, F.; van der Laan, G. X-ray circular dichroism as a probe of orbital magnetization. *Phys. Rev. Lett.* **1992**, *68*, 1943–1946.
- (27) Altarelli, M. Orbital-magnetization sum rule for x-ray circular dichroism: A simple proof. *Phys. Rev. B* **1993**, *47*, 597–598.

- (28) Oppeneer, P. Magneto-optical spectroscopy in the valence-band energy regime: relationship to the magnetocrystalline anisotropy. *J. Magn. Magn. Mater.* **1998**, *188*, 275–285.
- (29) Souza, I.; Vanderbilt, D. Dichroic f -sum rule and the orbital magnetization of crystals. *Phys. Rev. B* **2008**, *77*, 054438.
- (30) Yates, J. R.; Wang, X.; Vanderbilt, D.; Souza, I. Spectral and Fermi surface properties from Wannier interpolation. *Phys. Rev. B* **2007**, *75*, 195121.
- (31) Vanderbilt, D. *Berry phases in electronic structure theory: electric polarization, orbital magnetization and topological insulators*; Cambridge University Press: Cambridge, 2018.
- (32) Schüler, M.; De Giovannini, U.; Hübener, H.; Rubio, A.; Sentef, M. A.; Werner, P. Local Berry curvature signatures in dichroic angle-resolved photoelectron spectroscopy from two-dimensional materials. *Sci. Adv.* **2020**, *6*, eaay2730.
- (33) Resta, R. Magnetic circular dichroism versus orbital magnetization. *Phys. Rev. Research* **2020**, *2*, 023139.
- (34) Huang, Z.; Liu, Y.; Dini, K.; Tan, Q.; Liu, Z.; Fang, H.; Liu, J.; Liew, T.; Gao, W. Robust Room Temperature Valley Hall Effect of Interlayer Excitons. *Nano Lett.* **2020**, *20*, 1345–1351, 00017.
- (35) Kozin, V.; Shabashov, V.; Kavokin, A.; Shelykh, I. Anomalous Exciton Hall Effect. *Phys. Rev. Lett.* **2021**, *126*, 036801, 00003.
- (36) Zhao, W.; Ghorannevis, Z.; Chu, L.; Toh, M.; Kloc, C.; Tan, P.-H.; Eda, G. Evolution of Electronic Structure in Atomically Thin Sheets of WS₂ and WSe₂. *ACS Nano* **2013**, *7*, 791–797.

- (37) Rohlfing, M.; Louie, S. G. Electron-hole excitations and optical spectra from first principles. *Phys. Rev. B* **2000**, *62*, 4927.
- (38) Molina-Sánchez, A.; Sangalli, D.; Hummer, K.; Marini, A.; Wirtz, L. Effect of spin-orbit interaction on the optical spectra of single-layer, double-layer, and bulk MoS₂. *Phys. Rev. B* **2013**, *88*, 045412.
- (39) Zhu, B.; Chen, X.; Cui, X. Exciton Binding Energy of Monolayer WS₂. *Sci Rep* **2015**, *5*, 9218.
- (40) See Supporting Information at `tobeaddedbypublisher`.
- (41) Jackson, J. D. *Classical electrodynamics; 2nd ed.*; Wiley: New York, NY, 1975.
- (42) Li, Y.; Ludwig, J.; Low, T.; Chernikov, A.; Cui, X.; Arefe, G.; Kim, Y. D.; van der Zande, A. M.; Rigosi, A.; Hill, H. M.; Kim, S. H.; Hone, J.; Li, Z.; Smirnov, D.; Heinz, T. F. Valley Splitting and Polarization by the Zeeman Effect in Monolayer MoSe₂. *Phys. Rev. Lett.* **2014**, *113*, 266804.
- (43) Srivastava, A.; Sidler, M.; Allain, A. V.; Lembke, D. S.; Kis, A.; Imamoglu, A. Valley Zeeman effect in elementary optical excitations of monolayer WSe₂. *Nature Phys* **2015**, *11*, 141–147.
- (44) Stier, A. V.; McCreary, K. M.; Jonker, B. T.; Kono, J.; Crooker, S. A. Exciton diamagnetic shifts and valley Zeeman effects in monolayer WS₂ and MoS₂ to 65 Tesla. *Nat Commun* **2016**, *7*, 10643, 00002.
- (45) Li, Q. et al. Enhanced Valley Zeeman Splitting in Fe-Doped Monolayer MoS₂. *ACS Nano* **2020**, *14*, 4636–4645.
- (46) Li, W.; Lu, X.; Wu, J.; Srivastava, A. Optical control of the valley Zeeman effect through many-exciton interactions. *Nat. Nanotechnol.* **2021**, *16*, 148–152.

- (47) Gulans, A.; Kontur, S.; Meisenbichler, C.; Nabok, D.; Pavone, P.; Rigamonti, S.; Sagmeister, S.; Werner, U.; Draxl, C. exciting: a full-potential all-electron package implementing density-functional theory and many-body perturbation theory. *Journal of Physics: Condensed Matter* **2014**, *26*, 363202.
- (48) Vorwerk, C.; Aurich, B.; Cocchi, C.; Draxl, C. Bethe–Salpeter equation for absorption and scattering spectroscopy: implementation in the exciting code. *Electronic Structure* **2019**, *1*, 037001.
- (49) Perdew, J. P.; Burke, K.; Ernzerhof, M. Generalized Gradient Approximation Made Simple. *Phys. Rev. Lett.* **1996**, *77*, 3865–3868.